Ceramics International 48 (2022) 37114–37121

Contents lists available at ScienceDirect

Ceramics International

journal homepage: www.elsevier.com/locate/ceramint

3D calcium silicophosphate porous scaffold: *In vitro* and *in vivo* response

Patricia Ros-Tárraga [a], Carlos M. Martínez [b], Miguel A. Rodríguez [c], Piedad N. De Aza [a,*]

[a] Instituto de Bioingenieria, Universidad Miguel Hernández, Avd. Ferrocarril s/n, 03202, Elche, Alicante, Spain
[b] Instituto Murciano de Investigación Biosanitaria Virgen de la Arrixaca, Crta. Buenavista s/n, 03120, El Palmar, Murcia, Spain
[c] Instituto de Cerámica y Vidrio, ICV-CSIC, C/Kelsen 5, Madrid, 28049, Spain

ARTICLE INFO

Keywords:
Bone tissue engineering
Calcium silicophosphate
Ceramic scaffold
Mesenchymal stem cells
Biomaterial

ABSTRACT

The elderly population (65 years and older) is expected to increase from 524 million people in 2010 to 1.5 billion by 2050, with the corresponding increase in bone-related and joint damage problems. Many of these problems can be solved by using scaffolds for bone tissue regeneration, and material selection is a critical step to obtain satisfactory results. This selection is crucial for the cell division process, cell-cell communication pathways, nutrient transport and osteogenic differentiation. In this study, we designed a tridimensional porous ceramic scaffold composed of 85 wt%C_2S – 15 wt%TCP by the polymer sponge replica method combined with ceramic slurry, and we analyzed its biocompatibility and osteoinductive capacity by *in vitro* and *in vivo* assays. The *in vitro* tests showed good biocompatibility because the cells that were seeded over the biomaterial had spread over the entire surface. The *in vivo* results showed no cytotoxicity signs at the implant site, and the percentages of defect closure and residual biomaterial, and the resorption rate, were adequate. All these results demonstrate that 85 wt%C_2S – 15 wt%TCP bioceramics can be taken as potential bone substitutes to be employed for a range of medical applications.

1. Introduction

Bones are composed of inorganic crystals of hydroxyapatite an extracellular organic matrix, cells, lipids and water. This complex structure confers the skeleton ductility, strength and stiffness, which allow it to carry large loads and absorb impacts without breaking or deforming. Bones are also capable of self-regeneration when damaged thanks to modeling and remodeling processes [1,2]. These processes allow bones to change in size, shape and position during development and aging. Due to these physical changes, functional bone ability may also be modified. Mechanical weakening increases, bone stiffens and the cross-sectional area (trabecular surface over which the mechanical load is distributed) decreases with aging, which causes greater bone deformation that can lead to bone fractures in fragile bones [2].

The elderly population (≥65 years) has been growing for years now. Globally in 2010, 524 million people were 65 years or older, and this figure is expected to triple to around 1.5 billion by 2050 [3]. This is due to our society's longer life expectancy thanks to the health improvements achieved in recent times. However, this increase is associated with suffering more problems related to bone and joint damage.

Bone tissue regeneration requires the spreading, proliferation, migration, adhesion and differentiation of cells. Selecting material scaffolds with appropriate surface properties is critical for the cell division process, cell-cell communication pathways, nutrient transport and osteogenic differentiation [4–9]. Some of these processes can be regulated by surface topography and different inorganic ions, such as calcium (Ca), silicon (Si) and phosphorus (P), as described by the previous literature [10–13]. For this reason, calcium silicophosphate ceramics (CSC) are excellent candidates for developing 3D porous scaffolds. These ceramics can be obtained by several techniques like rapid prototyping, electrospinning processing, gel casting, the polymer replication method, among others [14]. A methodology based on polymer replication allows us to acquire porous 3D scaffolds that mimic human trabecular bone. Micropores and some mesopores bring about a larger surface area, which increases ion exchange and the bone-implant interaction, and macropores improve cell adhesion and migration to allow cell colonization and angiogenesis [15–18]. For both, bone formation and capillary in-growth purposes, the bibliography recommends macropores size exceeding 300 μm [19].

In this study, we designed a 3D hierarchical porous ceramic scaffold

* Corresponding author.
E-mail addresses: patricia.ros01@goumh.umh.es (P. Ros-Tárraga), cmmarti@um.es (C.M. Martínez), mar@icv.csic.es (M.A. Rodríguez), piedad@umh.es (P.N. De Aza).

https://doi.org/10.1016/j.ceramint.2022.08.287
Received 8 July 2022; Received in revised form 9 August 2022; Accepted 26 August 2022
Available online 31 August 2022

composed of 85 wt% dicalcium silicate (C_2S) – 15 wt% tricalcium phosphate (TCP), 85 wt%C_2S – 15 wt%TCP, by combining the polymer sponge replica and barbotine methodologies. Then materials' *in vitro* behavior was analyzed using adult human mesenquimal stem cells (ah-MSCs) and the *in vivo* response was studied with New Zealand rabbits.

2. Material and methods

The chemicals used in the synthesis of dicalcium silicate – tricalcium phosphate (C_2S – TCP) ceramic powders with a composition of 85 wt% C_2S – 15 wt%TCP were Ca-hydrogen phosphate anhydrous ($CaHPO_4$ > 98.0 wt% Panreac, Barcelona, Spain) and calcium carbonate ($CaCO_3$ > 99.0 wt% Fluka, St. Louis, MO, USA), with an average particle size of 13 μm and SiO_2 > 99.7 wt% (Strem Chemicals Inc., Newburyport, MA, USA), as the previous literature describes [20]. First a manual agate mortar was used to mix stoichiometric quantities of raw powders in acetone. A laboratory attrition miller was used to grind this mixture with 3 mm ∅ PSZ-Zirconia balls, using isopropyl alcohol as suspension media. Then, the powders mixture was isostatically pressed at 200 MPa to form a green body, which was heated in a platinum crucible at 1500 °C for 3 h at a heating rate of 12.5 °C/min. Next, samples were quenched with liquid nitrogen by being rapidly removed from the furnace. Then, the samples were ground and pressed again, and the final samples were sintered at 1500°C, with a heating rate of 8°C/min and with 5-h maintenance, followed by a temperature drop of 2.5 °C/min until 700 °C, 24-h maintenance at 700 °C and slow cooling until room temperature. These temperatures were selected following the C_2S – TCP phase equilibrium diagram [21].

To obtain the porous 3D ceramic scaffolds, a ceramic suspension was prepared using 55% solid content (85 wt%C_2S – 15 wt%TCP powders) and 45% water media. Then 2 wt% of defloculant (Dolapix CE-64, Zschimmer Schwartz, Germany) was employed in accordance with the previous literature [22]. Having obtained the ceramic slurry, polyurethane foams were immersed in barbotine ceramic suspension. Slurry excess was removed using compressed air to avoid plugging pores. Next, samples were sintered at a heating rate of 2 °C/min until a final temperature of 1350 °C was reached, which was maintained for 2 h. Temperature was lowered at a cooling rate of 2 °C/min until 500 °C and maintained for 7 h. Finally, samples were subjected to slow cooling to obtain the final 3D porous ceramic scaffolds.

A Nikon SMZ1500 stereomicroscope equipped, with a Nikon DXM1200F digital camera, was used to observe the macroscopic structure of the ceramic samples. A Scanning Electron Microscope (SEM, Hitachi S–3500 N) was employed to study samples' microstructure. They were covered with palladium, as previous literature describes [14].

To evaluate porous scaffolds' mineralogical composition, X-Ray Diffraction (XRD) patterns were obtained using a Bruker-AXS D8Advance automated diffractometer with CuKα 1.2 radiation (1.54056 Å). Data were collected in a Bragg-Brentano (θ/2θ) vertical geometry (flat reflection mode) between 20° and 50° (2θ) at 0.05° steps, with 6 s per step. The X-ray tube operated at 40 kV and 30 mA, as the previous literature describes [14]. The database provided by the Joint Committee on Powered Diffraction Standards (JCPDS) was employed to compare samples' diffractogram.

To determine the ceramic samples' structural composition, the Fourier Transform Infrared (FTIR) spectrum was obtained in a Thermo Scientific Nicolet iS5 equipped with an iD5 ATR Accessory. A spectrum was collected by employing 64 scans with a 4 cm^{-1} resolution at room temperature.

Inductively Coupled plasma Optical Emission Spectrometry (ICP-OES Perkin Elmer Optima 200™, Massachusetts, USA) was used to determine the ionic release of Ca, Si and P from the ceramic samples to the basal culture growth medium (GM). The GM comprised three products supplied by Sigma-Aldrich (St. Louis, MO, USA): Dubelcco's Modified Eagle Medium (DMEM); 10% Fetal Bovine Serum (FBS); 1% penicillin-streptomycin. Five pieces of porous ceramics (7 mm diameter, 4 mm thick) were sterilized in an autoclave at 121 °C and then placed in a 24-well plate with 1 mL of the GM per well. Samples were incubated at 37 °C in a 95% humidified atmosphere with 5% CO_2 for 1, 3 and 6 h, and for 1, 3, 7, 14, 21 and 28 days. Fresh GM was immediately added every time GM was collected and stored at 4 °C until ionic determination [23].

After analyzing ionic release, the cytotoxicity of this porous ceramic was evaluated by the lactate dehydrogenase assay (LDH Cytotoxicity Detection Kit, TAKARA, Tokyo, Japan). Porous scaffolds (4 mm diameter, 3 mm thick) were placed in a 48-well plate with 500 mL of the GM and 1% FBS to be incubated for 1 and 3 days at 37 °C in a 95% humidified atmosphere with 5% CO_2. Then, this medium (hereinafter referred to as the conditioned medium) was collected and stored at 4 °C. After waiting the necessary time to obtain the conditioned medium, 5,000 cells/cm^2 were seeded overnight in a 96-well plate with the GM. They were incubated for 1 day. After discarding the cellular medium, it was replaced with 200 μL of the conditioned medium and incubated for 1 day. Finally, following the manufacturer's protocol, 100 μL were collected to measure absorbance at 490 and 660 nm.

The cytotoxicity of the conditioned medium was compared to the spontaneous LDH release from the untreated cells (low control) and with the maximum LDH release by the cells treated with Triton X-100 (high control). The low control was composed of 200 μL of the GM with 1% FBS, while the high control comprised 100 μL of the GM with 1% FBS and 100 μL of Triton X-100 solution, prepared at 2% in the GM with 1% FBS.

Cell adhesion and morphology were studied by seeding 30,000 cells/scaffold in 48-well culture plates for 1, 7, 14, 21 and 28 days with the GM, which was replaced every 3 days. Prior to cell seeding, scaffolds were incubated with 5 μg/cm^2 of fibronectin from human plasma (Sigma-Aldrich, St. Louis, MO, USA) for 45 min. After each study time, the seeded ceramics were rinsed with phosphate buffer solution 1X (PBS 1X) and fixed for 1 h with 3% glutaraldehyde. After fixation, cells were conserved in 0.1 M cacodylate buffer until postfixation with 1% osmium tetroxide. Then samples were dehydrated in a gradient series of ethanol solutions (30%, 50%, 70%, 90%, 100% v/v). Critical point drying was undertaken with liquid CO_2. Finally, samples were observed by Field Emission Scanning Electron Microscopy (FESEM-Merlin™ VP Compact, Carl Zeiss Microscopy S.L., Oberkochen, Germany) after sputter-coating them with gold.

To finish the cell tests, the Alamar Blue assay was run to establish cellular viability (AB, Invitrogen, Carlsbad, CA, U.S.A.). Porous scaffolds were seeded with 5,000 cells/cm^2 in 48-well plates to be incubated with the GM for 1, 7, 14, 21 and 28 days. The medium was discarded after all the study times. Then PBS 1X was used to wash wells, which were then filled with 500 μL of the fresh GM and 10% v/v of the Alamar Blue reagent. The seeded ceramics were incubated at 37 °C in a 95% humidified atmosphere with 5% of CO_2 for 4 h in the dark. After this time, 200 μL of the dissolution were placed in a 96-well plate to take fluorescence measurements in a Synergy MX ultraviolet visible (UV–Vis) (Bio Tek Instuments Inc., Winooski, VT, USA) at the respective excitation and emission wavelengths of 560 nm and 590 nm. All the studies were run at least in triplicate. The results are expressed as arbitrary units (au).

To study the porous ceramics' *in vivo* behavior, six scaffolds (4 mm diameter, 3 mm thick) were implanted in six pathogen-free male New Zealand rabbits. The study protocol was examined and approved by the Institutional Ethics and Animal Experimentation Committee of the University Miguel Hernandez (Spain) according to Spanish Government Guidelines and European Community Guidelines for animal care (EU Directive 2010/63/EU for animal experiments, authorized No. 2018/VSC/PEA/00056 tipo2). Rabbits were 28–30 weeks old and weighed about 4–4.5 kg (skeletally mature to ensure growth plates or physis closure). Two tibial bone defects (5 mm diameter x 4 mm high) per animal were created. One of the defects was occupied by the porous scaffold and the other acted as the study control. The six animals were allocated randomly to two groups (n = 3 each) corresponding to two study periods: 1 and 3 months.

After a 2-3-week adaptation period, ceramics were implanted following the procedure previously described by our group [24,25]. The general anesthesia procedure employed ketamine hydrochloride (10 mg kg^{-1}, via i.m.) and the pre- and postoperative broad-spectrum antibiotic prophylaxis consisted in amoxycillin at 0.1 mL kg^{-1}, via i.m., single dose). After shaving surgical areas, they were washed with Betadine® antiseptic and an incision (5 mm diameter x 4 mm high) was made in the upper third of the anteromedial zone of tibias (metaphysis). This incision was made using a manual drill to prevent necrosis processes occurring. Before implanting ceramics, bone defects were thoroughly washed with saline solution to eliminate bone debris and any chips produced while creating the defect. Next, ceramics were introduced by press-fit (Fig. 1a) and the surgical wound was closed by performing an anatomical plane suture with resorbable sutures (Vicryl® 3/0). Finally, the wound was cleaned with Betadine® and a plastic dressing spray, Nobecutan®, was applied. Postoperative pain and inflammation were controlled with Buprenorphine at 0.3 mg kg^{-1} via i.m. twice daily for 4 days. Finally, rabbits were sacrificed after 1 and 3 months by intracardiac pentobarbital overdose (Dolethal®) to obtain tibias. The two tibias of each rabbit (one with the ceramic material, the other one as a control) were segmented and fixed in 4% buffered formalin (Panreac, Barcelona, Spain) for 72 h (Fig. 1b) to carry out the histological and histomorphometric analyses. Samples were decalcified for 7 days with a 21–23% (v/v) formic-acid-based solution (Shandon TBD2, Thermo Corp., Madrid, Spain), processed and paraffin-embedded. Four micrometer-thick transversal sections, laid perpendicularly to the bone axis, were stained by a standard hematoxylin and eosin protocol according to the literature [24].

All the stained sections were microscopically scanned (Pannoramic MIDI-II, 3D Histech, Budapest, Hungary) at 400X. The scaffold's individual regions of interest (ROIs) were manually selected to measure two different elements: residual implant and new bone tissue. The total surface of each was analyzed in all the microphotographs to calculate the total surface of each one by summing all the data in the microphotographs from all sections. A digital microscopy application was used to examine all the sections (Slide Viewer, Ver. 2.5, 3D Histech). Finally, manual measurements of ROIs were taken by a digital image analysis software (Zeiss ZEN, ver. 3.0, Carl Zeiss, Jenna, Germany) after calibrating the system and digitizing images.

The data from the assays are shown as the means ± standard deviation (SD) of at least three specimens per treatment condition. A Student's t-test was used to make a comparison between groups in the LDH and Alamar Blue assays. Any differences between the measured parameters in the histomorphometric analysis were studied by a Mann-Whitney nonparametric test. A p-value below 0.05 was considered to be statistically significant.

3. Results

Fig. 2 shows the porous 3D ceramic scaffolds fabricated with the polymer replica and the ceramic slurry composed of the 85 wt%C_2S – 15 wt%TCP ceramic powders. Fig. 2a–b depicts the macroscopic morphology of the porous scaffolds, and shows interconnected porosity and pores with uniform dimensions. This structure is confirmed by Fig. 2c–d, where we can see the microscopic morphology with the presence of elliptical pores, as well as the well-open porosity of samples with macropores of 300–600 μm (AB length) and 150–250 μm (CD length), and the whole surface is covered by micropores.

As microporosity (<40 μm pore size) and macroporosity (>100 μm pore size) in tissue engineering biomaterials are necessary for bone growth, the porosity control is the most important factor to control scaffold designs [26]. The macro- and microstructural analyses of the bioceramics showed a similar interconnected structure to natural cancellous bone [27] with pores bigger than 15 μm, which are needed to allow cell infiltration, and higher than 300 μm, which improves vascularization, nutrient diffusion and new tissue in-growth [28–30]. The roughness created by the structure's microporosity increases the biomaterial's surface contact, which improves cell adhesion and protein adsorption [31].

Both the XRD pattern and FTIR spectrum of the porous ceramics are found in Fig. 2e. Samples are monophasic and composed of $\alpha'C_2S_{ss}$ (JCPDS card no. 09–348). The FTIR spectrum shows the presence of the Si–O–Si, Si-O-NBO and PO_4^{3-} groups. Phosphate groups appeared in not only the region between 1000 and 1100 cm^{-1}, which correspond to asymmetric stretching vibration, but also in the band located at 586 cm^{-1} and corresponds to PO_4^{3-} bending vibration. The band located at 843 cm^{-1} was identified as the bending mode of the Si–O–Si groups, and that located at 882 cm^{-1} was associated with the stretching mode of the Si-O-NBO groups. To gain a better understanding of the results obtained from the FTIR spectrum, each IR frequency is associated with the different vibrational modes, which appear in Table 1.

The XRD spectra results of the 85 wt%C_2S - 15 wt%TCP bioceramic correspond to the monophasic phase of the starting material obtained by the solid-state reaction technique (data not shown), which agrees with the data obtained from the equilibrium phase in subsystem Ca_2SiO_4–$7CaOP_2O_52SiO_2$ in system Ca_2SiO_4 (C_2S) – tricalcium phosphate (TCP) [21] at temperatures below 800 °C, where only the $\alpha'C_2S_{ss}$ phase exists.

Changes in the Ca, Si and P ion concentration in the GM after the different immersion times of the 85 wt%C_2S – 15 wt%TCP samples are shown in Fig. 3a. The Ca ion concentration increased from 1 h to 3D with a value of 283 ±15 mg/L, before lowering at 7D and increasing again at 14D, with a maximum value of 314±20 mg/L. It continued to lower until the assay ended. Si ion behavior was similar to Ca for the early study times. It first increased until 14D and its maximum value was 85.08 ± 8 mg/L. Then, it remained constant until the study ended. Finally, the P ion concentration remained constant from 1 h to 6 h. Then it lowered from 33 ± 6 mg/L to 9 ± 2 mg/L at 7D, and then increased to 16 ± 3 mg/L during the last assay period. The pH values ranged from 7.54 to 7.65 (graphic not shown).

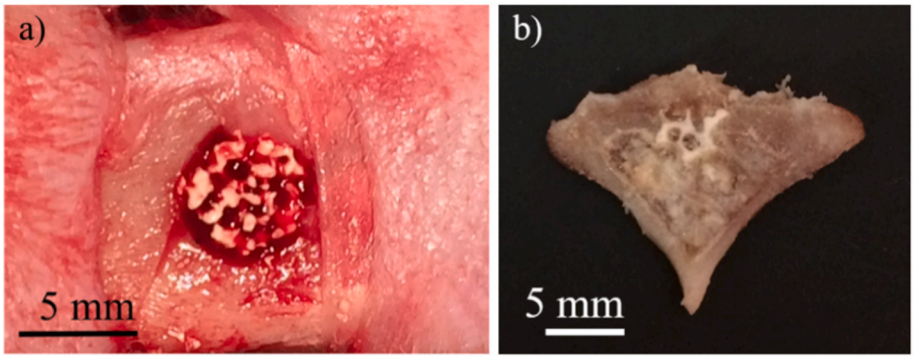

Fig. 1. a) Scaffold in the bone tissue defect, b) Bone segment with the implant 1 month after implantation, as a representative segment.

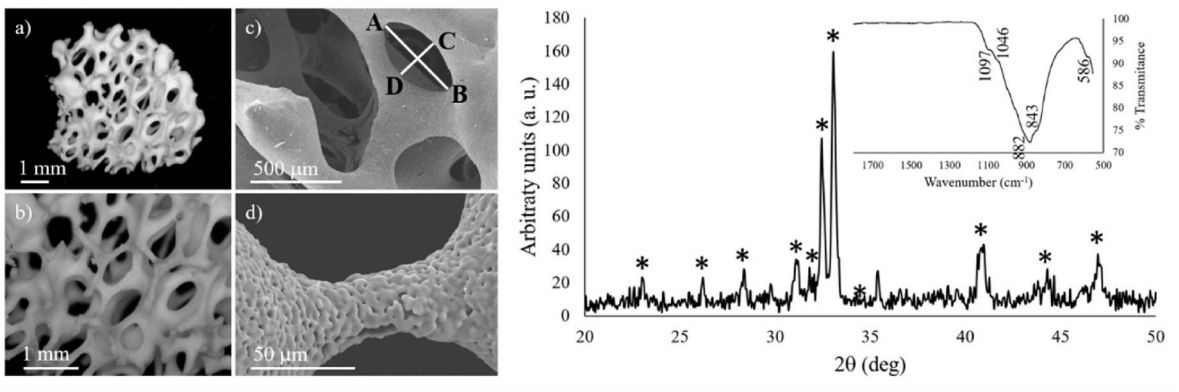

Fig. 2. a-b) Optical micrographs, c-d) SEM micrographs and e) the XRD pattern and the FTIR spectrum of the 85 wt%C_2S – 15 wt%TCP ceramics synthesized at 1350 °C.

Table 1
Infrared vibrational modes of the porous ceramics sintered at 1350 °C.

FTIR wave (cm^{-1})	Vibrational mode/group	Reference
500–600	PO_4^{3-} bending	[11,14,32]
760–850	Si–O–Si bending	[11,14,32]
890–975	Si-O-NBO stretching	[11,14,32]
1000–1100	PO_4^{3-} asymmetric stretching	[11,14,32]

Ca phosphate biomaterials are widely accepted for bone tissue regeneration thanks to their good biocompatibility, osseointegration and osteoconduction [33]. It is known that Si plays a central role in physiological bone tissue formation, particularly given its ability to favor the precipitation of hydroxyapatite (HA) and bone mineralization [34]. For these reasons, the effect of the dissolution of the scaffolds composed of 85 wt%C_2S – 15 wt%TCP when immersed in DMEM should be studied in cytotoxicity, cell adhesion and proliferation terms.

Fig. 3b offers the LDH quantification results. The cells without any material (low control) obtained 11 ± 2%% spontaneous cell death. When 85 wt%C_2S – 15 wt%TCP were immersed in the GM for 1 day, the ionic release from the material induced 11 ± 2% cell death. When this time was prolonged to 3 days, the ionic release from the ceramic material induced 8 ± 2% cell death. Both results showed no significant differences with the low control, which means that this ceramic material, composed by 85 wt%C_2S – 15 wt% TCP, is not cytotoxic for ah-MSCs.

The adhesion, morphology, proliferation and metabolic activity of the ah-MSCs seeded on 85 wt%C_2S – 15 wt%TCP are shown in Fig. 4. After only 1-day incubation in the GM, the porous ceramic surface was covered by small calcium phosphate nodules and cells had completely spread out. At 7 days, the number of cells increased and covered most of the surface. After 21 days and 28 days, cells completely covered the surface by a uniform monolayer, even pores, and showed their characteristic branched random morphology of ah-MSCs. The numerous created filopodia, which enhanced their adhesion and contact surface with the porous ceramic, allowed new connections to be made with the adjacent cells. It was not easy to recognize individual cells at this point and no cytotoxicity signs were noted at any study time; e.g. lysis, cell detachment, changes in membrane integrity (Fig. 4a).

Fig. 4b shows the viability and metabolic activity of the ah-MSCs incubated in contact with the porous ceramics. The AB fluorescence measurements taken after 1, 7, 14, 21 and 28 days in the GM are displayed. Both, the control and material cells (cells seeded on tissue culture polystyrene, TCPS, and porous ceramic, respectively) showed enhanced cell metabolic activity with time, which indicates the good viability of the cells in contact with the ceramic material. There were some significant differences ($p < 0.05$) between the control and material cells during early study periods, although no significant differences appeared in the fluorescence values between the control and material cells at 21 and 28 days, and the values of both were high.

The AB results showed bioceramics' biocompatibility because no significant differences were observed at 21 and 28 days between the control and material cells. However, early study times (1 and 7 days), cells did not show any incremented cell metabolic activity, which may be explained by ah-MSCs' self-renewal capacity, a property that is associated with growth and proliferation properties [12]. Cells need time to adapt and proliferate because the porous bioceramic is a new environment for them.

The 1-month postsurgery histopathological analysis showed slight cortical bone closure in the control animals (Fig. 5a, bidirectional arrow

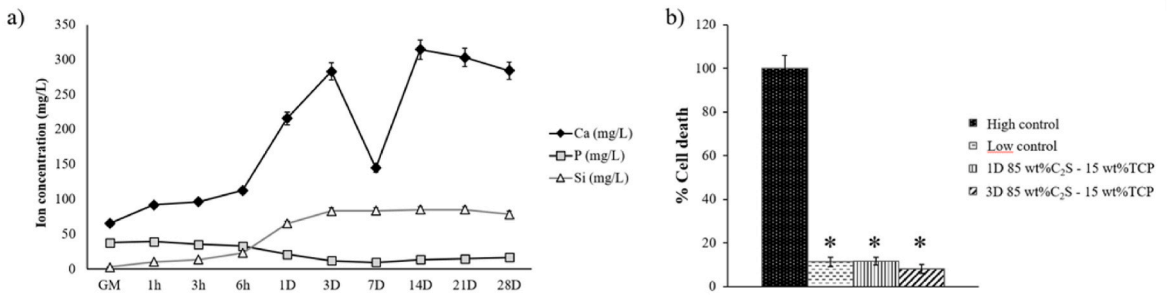

Fig. 3. a) Ca, P and Si ion concentrations of the GM, as a control, and the GM after immersing the 85 wt%C_2S – 15 wt%TCP porous ceramics for 1, 3, 6 h and 1, 3, 7, 14, 21 and 28 days (1 h, 3 h, 6 h, 1D, 3D, 7D, 14D, 21D and 28D); b) Cytotoxicity of the material in cell death percentage terms after 1 and 3 days (1D and 3D). The maximum LDH release acted as the high control and the spontaneous LDH release from cells as the low control. * means significant differences ($p < 0.05$) between the high control and the other measurements.

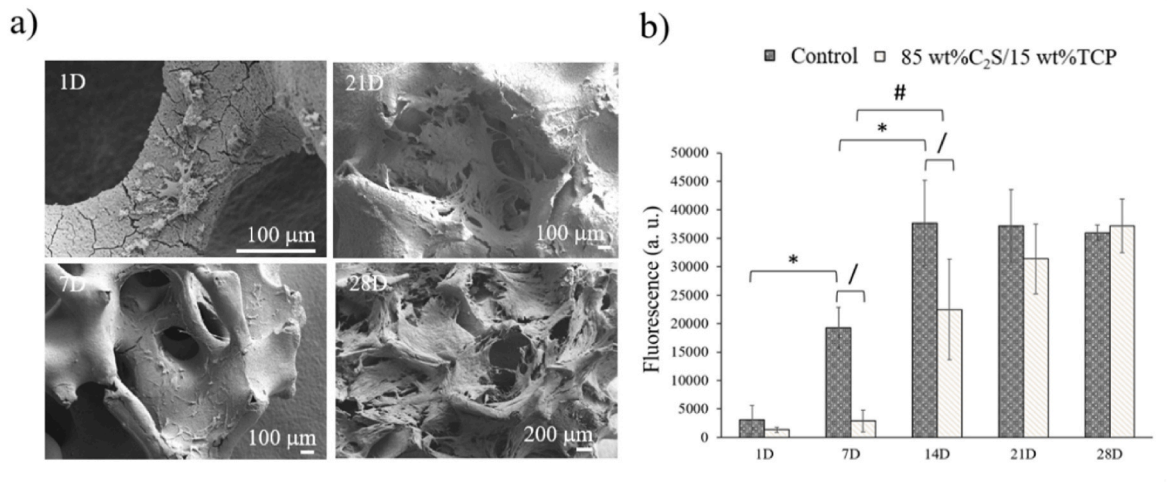

Fig. 4. Representative FESEM images of the ah-MSCs seeded on the surface of the 85 wt%C_2S – 15 wt%TCP bioceramics after a) 1 day, 7 days, 21 days and 28 days (1D, 7D, 21D and 28D) with the GM, and b) cellular metabolic activity of the cells in contact with the porous ceramic compared with cells in TCPS (positive control). * means significant differences ($p < 0.05$) between TCPS cells during different time periods. # means significant differences ($p < 0.05$) between porous ceramic cells during different time periods./means significant differences ($p < 0.05$) between porous ceramic and TCPS cells during the same experimental time.

and Table 2), microscopically characterized by the presence of numerous bone trabeculae (Fig. 5a, T) with no organized pattern and prominent bone callus formation (Fig. 5a, BC), and histological evidence for condrogenic differentiation (Fig. 5a, C) during endochondral ossification transition (Fig. 5a, EO). The neoformed trabeculae located in the cortical bone (Fig. 5b) showed immature lamellar bone (Fig. 5b, asterisk) and well-vascularized (Fig. 5b, V) connective tissue (Fig. 5b, CT) with numerous active osteoblasts (Fig. 5b, head arrows) that configured the neoformed bone.

The animals with the intraosseous biomaterial implant showed more prominent defect closure (Fig. 5c, bidirectional arrow) than the control animals (Table 2), and more organized neoformed cortical bone with fewer bone trabeculae (Fig. 5c, T) and less prominent bone callus (Fig. 5c, BC). The presence of the biomaterial (Fig. 5c, B) can be microscopically detected in both cortical and medullary bone. At higher magnification (Fig. 5d), the neoformed lamellar bone had completely developed (Fig. 5d, asterisk) with a few bone trabeculae (Fig. 5d, T), and also with the same histological characterization described in the control animals. The cortical zone, which was still closing (Fig. 5e), displayed granulation tissue (Fig. 5e, GT), which can be considered a precursor to new bone formation. It was surrounded by lamellar bone trabeculae (Fig. 5e, T) with many osteoblasts (Fig. 5e, head arrow). At the medullary level (Fig. 5f), well-vascularized granulation tissue was observed (Fig. 5d, GT) with a discrete inflammatory infiltrate (Fig. 5f, I) composed mainly of macrophages and biomaterial deposits (Fig. 5f, B), some with histological trabecular bone neoformation features (Fig. 5f, T) and lots of active osteoblasts (Fig. 5f, head arrow).

At 3-month postsurgery, cortical closure complete was observed in the control animals (Fig. 5g, CC). At higher magnification (Fig. 5h), cortical bone showed fully developed lamellar bone (Fig. 5h, asterisk), and some points of endochondral ossification were still detected (Fig. 5h, EO).

The cortical closure in the animals with the intraosseous biomaterial implant at 3-month postsurgery was also complete (Fig. 5i, CC). At higher magnification (Fig. 5j), cortical bone showed well-developed lamellar bone (Fig. 5j, asterisk) with some points of endochondral ossification (Fig. 5j, EO), similarly to those described in the control animals. Interestingly, these animals presented lamellar bone formation in the medulla (Fig. 5k, asterisk) and the discrete presence of biomaterial deposits (Fig. 5k, B).

The *in vivo* assays demonstrated properties of bioceramic stimulate bone tissue regeneration. When we looked at the results obtained for the bone to implant contact (%), we observed a drop in the percentage from 8 ± 3% in the animals with intraosseous biomaterial at 1 month postsurgery to 7 ± 1% in the animals with intraosseous biomaterial at 3 months postsurgery. For the percentage of defect closure 1 month after surgery, the animals with the intraosseous biomaterial showed a higher value than the control animals (44 ± 10% and 30 ± 1%, respectively). This finding indicates that the biomaterial is capable of accelerating bone tissue regeneration. All the animals showed complete defect closure 3 months after surgery. Finally, the results obtained from the percentages of the resorption rate and residual biomaterial revealed that bioceramics were biodegradable. The percentage of the resorption rate rose by approximately 17% when the postsurgery time increased from 1 to 3 months (60 ± 13% and 77 ± 4%, respectively), which agrees with the results obtained for the percentage of residual biomaterial showing a drop in percentage when the postsurgery time was prolonged from 1 to 3 months (30 ± 4% and 21 ± 5%, respectively).

This research demonstrates that the bioceramics are capable of mimicking bone tissue, and osteoblasts are able to adhere and proliferate over their surface better than with other materials. Calcium phosphate ceramics (CPC) have been profoundly studied for bone tissue engineering because of its physico-chemical properties, osteoconduction and osteoinduction. For these reasons, improvements in the different properties of CPCs, such as compressive strength, biodegradability, bioactivity, solubility, surface topography, among others, have been the focus of different studies in recent years [35,36]. Extremely biodegradable materials are excellent candidates for bone tissue engineering. However, an equilibrium between new bone growth and the material degradation rate is essential for creeping substitution, where a slow near-complete graft resorption must take place with simultaneous new bone deposition [37]. CPCs' biodegradability can be improved by combining them with ceramics composed of Si, like C_2S, which lower a materials' resorption rate and speed up bone regeneration to well contribute to creeping substitution. The results obtained in the present work reveal a progressive resorption rate for the bioceramics, which allows whole scaffold colonization and the formation of new bone around and inside it.

4. Conclusions

Porous $\alpha'C_2S_{ss}$ monophasic scaffolds composed of 85 wt%C2S – 15 wt %TCP were fabricated by immersing polyurethane sponges in ceramic slurry and following a sintering process in accordance with the C_2S-TCP

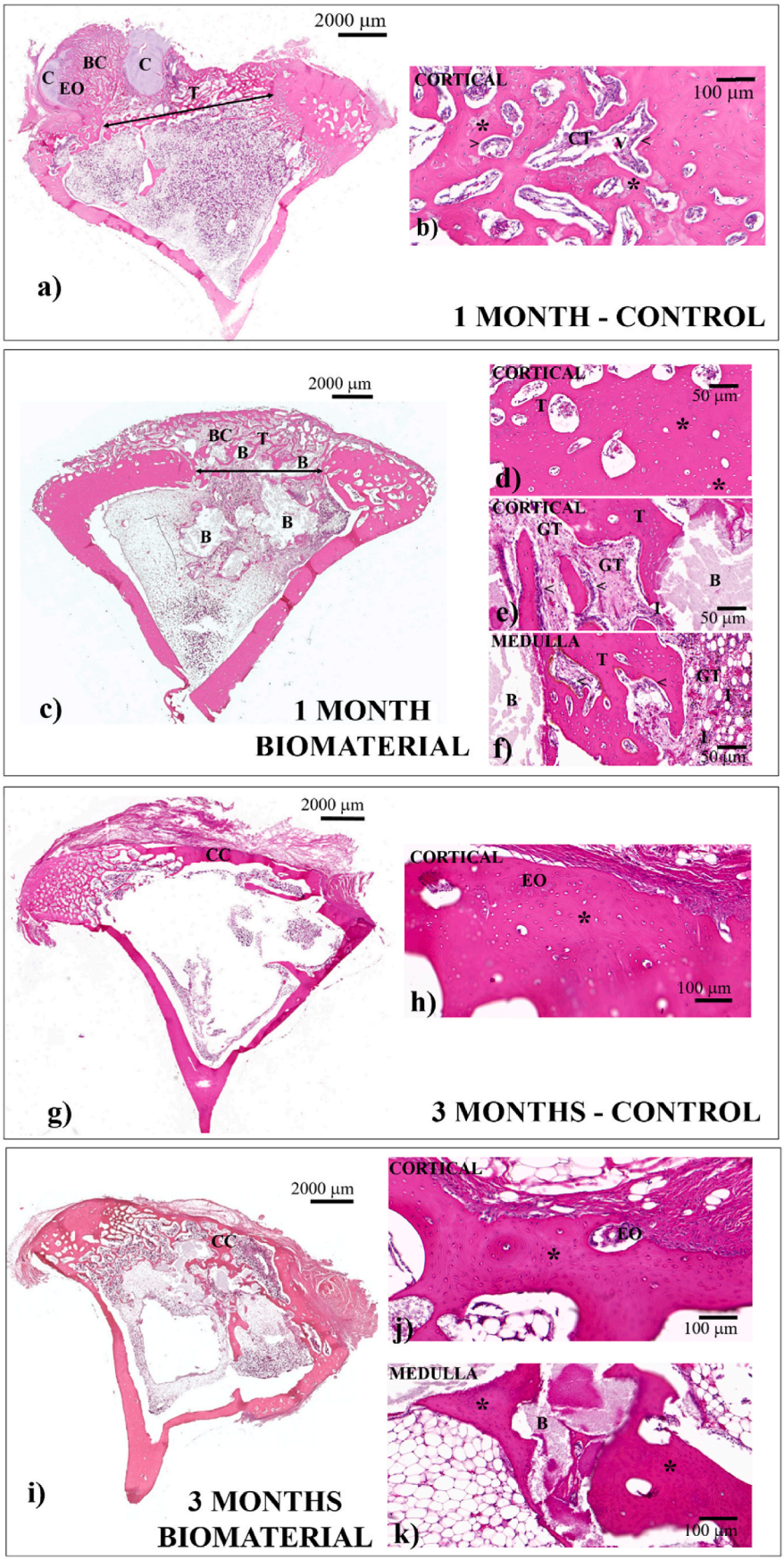

Fig. 5. a) Representative image of a 1-month post-surgery tibia sample of a control animal; b) Detailed image of the characteristic bone structures of a 1-month post-surgery tibia sample of a control animal; c) Representative image of a 1-month post-surgery tibia sample of an animal with the intraosseous biomaterial implant; d-f) Detailed images of the characteristic bone structures of a 1-month post-surgery tibia sample of an animal with the intraosseous biomaterial implant; g) Representative image of a 3-month post-surgery tibia sample of a control animal; h) Detailed image of the characteristic bone structures of a 3-month post-surgery tibia sample of a control animal; i) Representative image of a 3-month post-surgery tibia sample of an animal with the intraosseous biomaterial implant; j-k) Detailed images of the characteristic bone structures of a 3-month post-surgery tibia sample of an animal with the intraosseous biomaterial implant. C = Condrogenic differentiation; EO = Endochondral ossification; BC = Bone callus; T = Bone trabeculae; > and ≤ Active osteoblasts; CT = Connective tissue; V = Vascularized tissue; * = Lamellar bone; Bidirectional arrow = Closure of cortical bone; B = Biomaterial; GT = Granulation tissue; I = Inflammatory infiltrate; CC = Complete cortical closure.

Table 2
Histomorphometrical analysis of the animals with the biomaterial versus the control animals after 1 month and 3 months postsurgery. * means significant differences ($p < 0.05$) between the animals with the biomaterial at 1 and 3 months postsurgery. # means significant differences ($p < 0.05$) between the animals with the biomaterial and the control animals 1 month after surgery.

	1 month postsurgery - Biomaterial	1 month postsurgery - Control	3 months postsurgery - Biomaterial	3 months postsurgery - Control
BONE TO IMPLANT CONTACT (%)	**8 ± 3**	-	**7 ± 1**	-
DEFECT CLOSURE (%)	**44 ± 10#**	**30 ± 1#**	**100 ± 0**	**100.00 ± 0**
RESIDUAL BIOMATERIAL (%)	**30 ± 4***	-	**21 ± 5***	-
RESORPTION RATE (%)	**60 ± 13***	-	**77 ± 4***	-

phase equilibrium diagram. The results of the *in vitro* tests using ah-MSCs seeded directly on the material showed bioceramics' excellent biocompatibility because cells had spread over the entire surface, and even covered the biggest porous structure, at an adequate proliferation rate.

The 85 wt%C_2S – 15 wt%TCP ceramic scaffolds are capable of accelerating bone defect closure only 1 month after surgery compared to the control animals, which contributes to bone regeneration. Furthermore, the resorption rate recorded for the biomaterial is higher and directly proportional to the postsurgery time. This fact, together with the noncytotoxic effects observed in both the *in vitro* and *in vivo* assays, demonstrate that these bioceramics are biodegradable and innocuous for humans. All these results demonstrate that 85 wt%C_2S – 15 wt%TCP ceramics are potential bone tissue engineering candidates.

Formatting of funding sources

The authors acknowledge support from the Grant PID2020-116693RB-C21 funded by MCIN/AEI/10.13039/501100011033.

CRediT authorship contribution statement

Patricia Ros-Tárraga: Methodology, Writing – original draft, Formal analysis. **Carlos M. Martínez:** Methodology, Formal analysis. **Miguel A. Rodríguez:** Methodology. **Piedad N. De Aza:** Funding acquisition, Investigation.

Declaration of competing interest

The authors declare that they have no known competing financial interests or personal relationships that could have appeared to influence the work reported in this paper.

References

[1] Department of Health and Human Services, The basics of bone in health and disease, Bone Health and Osteoporosis: A Report of the Surgeon General, 2004, pp. 1–437. PMID: 20945569, http://www.surgeongeneral.gov/library.
[2] A.L. Boskey, R. Coleman, Aging and bone, J. Dent. Res. 89 (2010) 1333–1348, https://doi.org/10.1177/0022034510377791.
[3] C.J.P. Colón, I.L. Molina-Vicenty, M. Frontera-Rodríguez, A. García-Ferré, B. P. Rivera, G. Cintrón-Vélez, S. Frontera-Rodríguez, Muscle and bone mass loss in the elderly population: advances in diagnosis and treatment, J. Biomed. (Syd) 3 (2018) 40, https://doi.org/10.7150/jbm.23390.
[4] R. Eivazzadeh-Keihan, K.K. Chenab, R. Taheri-Ledari, J. Mosafer, S.M. Hashemi, A. Mokhtarzadeh, A. Maleki, M.R. Hamblin, Recent advances in the application of mesoporous silica-based nanomaterials for bone tissue engineering, Mater. Sci. Eng. C (2019), 110267, https://doi.org/10.1016/j.msec.2019.110267.
[5] C. Domingues-Faria, M.-P. Vasson, N. Goncalves-Mendes, Y. Boirie, S. Walrand, Skeletal muscle regeneration and impact of aging and nutrition, Ageing Res. Rev. 26 (2016) 22–36, https://doi.org/10.1016/j.arr.2015.12.004.
[6] J.M. Grasman, M.J. Zayas, R.L. Page, G.D. Pins, Biomimetic scaffolds for regeneration of volumetric muscle loss in skeletal muscle injuries, Acta Biomater. 25 (2015) 2–15, https://doi.org/10.1016/j.actbio.2015.07.038.
[7] M. Grellier, L. Bordenave, J. Amedee, Cell-to-cell communication between osteogenic and endothelial lineages: implications for tissue engineering, Trends Biotechnol. 27 (2009) 562–571, https://doi.org/10.1016/j.tibtech.2009.07.001.
[8] E.A. Botchwey, M.A. Dupree, S.R. Pollack, E.M. Levine, C.T. Laurencin, Tissue engineered bone: measurement of nutrient transport in three-dimensional matrices, J. Biomed. Mater. Res. 67 (2003) 357–367, https://doi.org/10.1002/jbm.a.10111.
[9] B. Kasemo, Biological surface science, Surf. Sci. 500 (2002) 656–677, https://doi.org/10.1016/S0039-6028(01)01809-X.
[10] P. Ros-Tárraga, N.A. Mata, Á. Murciano, P. Velasquez, P.N. De Aza, Multilayer ceramic materials: a method to link bioactivity and durability, Ceram. Int. 45 (2019) 23611–23618, https://doi.org/10.1016/j.ceramint.2019.08.072.
[11] N.A. Mata, P. Ros-Tárraga, P. Velasquez, A. Murciano, P.N. De Aza, Synthesis and characterization of 3D multilayer porous Si–Ca–P scaffolds doped with Sr ions to modulate in vitro bioactivity, Ceram. Int. 46 (2020) 968–977, https://doi.org/10.1016/j.ceramint.2019.09.058.
[12] P. Ros-Tárraga, P. Mazón, B. Revilla-Nuin, R. Rabadán-Ros, P.N. De Aza, L. Meseguer-Olmo, High temperature CaSiO3–Ca3 (PO4) 2 ceramic promotes osteogenic differentiation in adult human mesenchymal stem cells, Mater. Sci. Eng. C 107 (2020), 110355, https://doi.org/10.1016/j.msec.2019.110355.
[13] P. Mazón, D. García-Bernal, L. Meseguer-Olmo, F. Cragnolini, P.N. De Aza, Human mesenchymal stem cell viability, proliferation and differentiation potential in response to ceramic chemistry and surface roughness, Ceram. Int. 41 (2015) 6631–6644, https://doi.org/10.1016/j.ceramint.2015.01.110.
[14] P. Ros-Tárraga, A. Murciano, P. Mazón, S.A. Gehrke, P.N. De Aza, New 3D stratified Si-Ca-P porous scaffolds obtained by sol-gel and polymer replica method: microstructural, mineralogical and chemical characterization, Ceram. Int. 43 (2017) 6548–6553, https://doi.org/10.1016/j.ceramint.2017.02.081.
[15] C. Navalón, P. Mazón, P.N. De Aza, Eutectoid dicalcium silicate-Nurse's A ceramic scaffold: processing and in vitro bioactivity, Ceram. Int. 45 (2019) 21716–21724, https://doi.org/10.1016/j.ceramint.2019.07.172.
[16] C.M. Murphy, M.G. Haugh, F.J. O'brien, The effect of mean pore size on cell attachment, proliferation and migration in collagen–glycosaminoglycan scaffolds for bone tissue engineering, Biomaterials 31 (2010) 461–466, https://doi.org/10.1016/j.biomaterials.2009.09.063.
[17] K.-S. Lew, R. Othman, K. Ishikawa, F.-Y. Yeoh, Macroporous bioceramics: a remarkable material for bone regeneration, J. Biomater. Appl. 27 (2012) 345–358, https://doi.org/10.1177/0885328211406459.
[18] H. Niu, D. Lin, W. Tang, Y. Ma, B. Duan, Y. Yuan, C. Liu, Surface topography regulates osteogenic differentiation of MSCs via crosstalk between FAK/MAPK and ILK/β-catenin pathways in a hierarchically porous environment, ACS Biomater. Sci. Eng. 3 (2017) 3161–3175, https://doi.org/10.1021/acsbiomaterials.7b00315.
[19] M.J. Gupte, W.B. Swanson, J. Hu, X. Jin, H. Ma, Z. Zhang, Z. Liu, K. Feng, G. Feng, G. Xiao, Pore size directs bone marrow stromal cell fate and tissue regeneration in nanofibrous macroporous scaffolds by mediating vascularization, Acta Biomater. 82 (2018) 1–11, https://doi.org/10.1016/j.actbio.2018.10.016.
[20] P.N. De Aza, F. Zuleta, P. Velasquez, N. Vicente-Salar, J.A. Reig, a`$_H$-Dicalcium silicate bone cement doped with tricalcium phosphate: characterization, bioactivity and biocompatibility, J. Mater. Sci. Mater. Med. 25 (2014) 445–452.
[21] V. Rubio, M.A. de la Casa-Lillo, S. De Aza, P.N. De Aza, The system $Ca_3(PO_4)_2$ – Ca_2SiO_4: the sub-system Ca_2SiO_4 – $7CaOP_2O_52SiO_2$, J. Am. Ceram. Soc. 94 (2011) 4459–4462.
[22] C. Navalón, P. Ros-Tárraga, A. Murciano, P. Velasquez, P. Mazón, P.N. De Aza, Easy manufacturing of 3D ceramic scaffolds by the foam replica technique combined with sol-gel or ceramic slurry, Ceram. Int. 45 (2019) 18338–18346, https://doi.org/10.1016/j.ceramint.2019.06.048.
[23] R. Rabadan-Ros, P. Mazón, S. Serena, M. Sainz, L. Meseguer-Olmo, P.N De Aza, In vitro behaviour of Nurse's Ass-phase: a new calcium silicophosphate ceramic, J. Eur. Ceram. Soc. 37 (2017) 2943–2952.
[24] A. Parrilla-Almansa, N. García-Carrillo, P. Ros-Tárraga, C. Martínez, F. Martínez-Martínez, L. Meseguer-Olmo, P.N. De Aza, Demineralized bone matrix coating Si-Ca-P ceramic does not improve the osseointegration of the scaffold, Materials 11 (2018) 1580.
[25] P. Ros-Tárraga, P. Mazón, M.A. Rodríguez, L. Meseguer-Olmo, P.N. De Aza, Novel resorbable and osteoconductive calcium silicophosphate scaffold induced bone formation, Materials 9 (2016) 785, https://doi.org/10.3390/ma9090785.
[26] R. Agarwal, A.J. García, Biomaterial strategies for engineering implants for enhanced osseointegration and bone repair, Adv. Drug Deliv. Rev. 94 (2015) 53–62, https://doi.org/10.1016/j.addr.2015.03.013.
[27] A. Diaz-Arca, P. Ros-Tarraga, M.J.M. Tome, A.H. De Aza, L. Meseguer-Olmo, P. Mazon, P.N. De Aza, Micro-/Nano-Structured ceramic scaffolds that mimic natural cancellous bone, Materials 14 (2021), https://doi.org/10.3390/ma14061439.
[28] T. Freyman, I. Yannas, L. Gibson, Cellular materials as porous scaffolds for tissue engineering, Prog. Mater. Sci. 46 (2001) 273–282, https://doi.org/10.1016/S0079-6425(00)00018-9.
[29] J. Lu, B. Flautre, K. Anselme, P. Hardouin, A. Gallur, M. Descamps, B. Thierry, Role of interconnections in porous bioceramics on bone recolonization in vitro and in vivo, J. Mater. Sci. Mater. Med. 10 (1999) 111–120, https://doi.org/10.1023/a:1008973120918.

[30] D.W. Hutmacher, J.T. Schantz, C.X.F. Lam, K.C. Tan, T.C. Lim, State of the art and future directions of scaffold-based bone engineering from a biomaterials perspective, J. Tissue Eng. Regen. Med. 1 (2007) 245–260, https://doi.org/10.1002/term.24.
[31] B. Majhy, P. Priyadarshini, A. Sen, Effect of surface energy and roughness on cell adhesion and growth–facile surface modification for enhanced cell culture, RSC Adv. 11 (2021) 15467–15476, https://doi.org/10.1039/d1ra02402g.
[32] H. Aguiar, J. Serra, P. González, B. León, Structural study of sol–gel silicate glasses by IR and Raman spectroscopies, J. Non-Cryst. Solids 355 (2009) 475–480, https://doi.org/10.1016/j.jnoncrysol.2009.01.010.
[33] N. Eliaz, N. Metoki, Calcium phosphate bioceramics: a review of their history, structure, properties, coating technologies and biomedical applications, Materials 10 (2017), https://doi.org/10.3390/ma10040334.
[34] M. Tavoni, M. Dapporto, A. Tampieri, S. Sprio, Bioactive calcium phosphate-based composites for bone regeneration, J. Compos. Sci. 5 (2021) 227, https://doi.org/10.3390/jcs5090227.
[35] T. Ghassemi, A. Shahroodi, M.H. Ebrahimzadeh, A. Mousavian, J. Movaffagh, A. Moradi, Current concepts in scaffolding for bone tissue engineering, Archives of bone and joint surgery 6 (2018) 90. PMID: 29600260.
[36] I. Martinez, P. Velasquez, P. De Aza, Synthesis and stability of α-tricalcium phosphate doped with dicalcium silicate in the system Ca3 (PO4) 2–Ca2SiO4, Mater. Char. 61 (2010) 761–767, https://doi.org/10.1016/j.matchar.2010.04.010.
[37] T.T. Roberts, A.J. Rosenbaum, Bone grafts, bone substitutes and orthobiologics: the bridge between basic science and clinical advancements in fracture healing, Organogenesis 8 (2012) 114–124, https://doi.org/10.4161/org.23306.